

# Calculation of renormalized viscosity and resistivity in magnetohydrodynamic turbulence

Mahendra K. Verma \*

*Department of Physics, Indian Institute of Technology, Kanpur – 208016, INDIA*

(May 2001)

A self-consistent renormalization (RG) scheme has been applied to nonhelical magnetohydrodynamic turbulence with normalized cross helicity  $\sigma_c = 0$  and  $\sigma_c \rightarrow 1$ . Kolmogorov's 5/3 powerlaw is assumed in order to compute the renormalized parameters. It has been shown that the RG fixed point is stable for  $d \geq d_c \approx 2.2$ . The renormalized viscosity  $\nu^*$  and resistivity  $\eta^*$  have been calculated, and they are found to be positive for all parameter regimes. For  $\sigma_c = 0$  and large Alfvén ratio (ratio of kinetic and magnetic energies)  $r_A$ ,  $\nu^* = 0.36$  and  $\eta^* = 0.85$ . As  $r_A$  is decreased,  $\nu^*$  increases and  $\eta^*$  decreases, until  $r_A \approx 0.25$  where both  $\nu^*$  and  $\eta^*$  are approximately zero. For large  $d$ , both  $\nu^*$  and  $\eta^*$  vary as  $d^{-1/2}$ . The renormalized parameters for the case  $\sigma_c \rightarrow 1$  are also reported.

PACS numbers: 47.27.Gs, 52.35.Ra, 11.10.Gh

## I. INTRODUCTION

The Renormalization Group (RG) technique provided an important tool for understanding of the phenomena of phase transitions and critical phenomena. Motivated by this success, researchers have applied this technique to turbulence and other nonequilibrium systems. In this paper we apply RG to magnetohydrodynamic (MHD) turbulence.

Forster *et al.* [1] first applied dynamical RG procedure to the analysis of Navier-Stokes and Burgers equations, both stirred by random forces. They eliminated the large-wavenumber modes and included the effects of nonlinearity in the effective viscosity. Later, DeDominicis and Martin [2], Fournier and Frisch [3], Yakhot and Orszag [4], many others studied various aspects of RG for fluid turbulence, but all of them considered certain form of external forcing. McComb and his coworkers ([5,6] and reference therein) instead applied self-consistent RG procedure; here the energy spectrum was assumed to be Kolmogorov's spectrum, and the renormalized viscosity was computed iteratively. We have adopted a similar scheme for MHD turbulence.

Fournier *et al.* [7], Camargo and Tasso [8], and Liang and Diamond [9] employed RG technique to MHD turbulence on the similar lines as adopted by Forster *et al.* [1] for fluid turbulence. Fournier *et al.* [7] found that for  $d > d_c \approx 2.8$ , there are two nontrivial regimes: a kinetic regime where the renormalization of the transport coefficients is due to kinetic small-scales; and a magnetic regime where it is due to the magnetic small-scales. In dimensions  $2 \leq d \leq d_c$ , there is no stable fixed point for turbulence with sufficiently strong external currents. Camargo and Tasso [8] studied the effective (renormalized) viscosity and resistivity and concluded that negative viscosity and resistivity are not permissible except in certain cases. Liang and Diamond [9] showed that no RG fixed point exists in 2D MHD turbulence. All the above authors however do not give any clear idea about the energy spectrum of MHD turbulence, which still remains controversial. However, Verma [10] used technique similar to that of McComb and Coworkers ([5,6] and references therein) and showed that Kolmogorov's spectrum is a consistent solution of MHD RG equations.

Kraichnan [11] and Iroshnikov [12] first gave phenomenology of steady-state, homogeneous, and isotropic MHD turbulence. They argued that the kinetic and magnetic energy spectra ( $E^u(k)$  and  $E^b(k)$  respectively) are

$$E^u(k) = E^b(k) = A(\Pi B_0)^{1/2} k^{-3/2} \quad (1.1)$$

where  $\Pi$  is the total energy cascade rate,  $B_0$  is the mean magnetic field or the magnetic field of the largest eddy, and  $A$  is a universal constant of order one. Later Matthaeus and Zhou [13], and Zhou and Matthaeus [14] proposed a

---

\*email: mkv@iitk.ac.in

generalized phenomenology in which the cascade rates  $\Pi^\pm$  and energy spectra  $E^\pm(k)$  of Elsässer variables  $\mathbf{z}^\pm (= \mathbf{u} \pm \mathbf{b})$  are related by

$$\Pi^\pm = \frac{A^2 E^+(k) E^-(k) k^3}{B_0 + \sqrt{k E^\pm(k)}} \quad (1.2)$$

where  $A$  is a constant. In the limit  $B_0 = 0$ , we can immediately obtain

$$E^\pm(k) = K^\pm \frac{(\Pi^\pm)^{4/3}}{(\Pi^\mp)^{2/3}} k^{-5/3} \quad (1.3)$$

where  $K^\pm$  are Kolmogorov's constants for MHD. The Eq. (1.3) was first derived by Marsch [15].

The energy spectrum of the solar wind, a well known observational platform for MHD turbulence, is closer to  $k^{-5/3}$  than to  $k^{-3/2}$  [16,17]. In addition, the recent numerical [18–20] and theoretical [10,21,22] work support Kolmogorov-like phenomenology for MHD turbulence. Curiously, Kolmogorov's spectrum is observed even in the presence of a mean magnetic field. To understand theoretically, Verma [10], Sridhar and Goldreich [21], and Goldreich and Sridhar [22] applied field theoretic techniques to MHD turbulence. Verma [10] showed that the mean magnetic field  $B_0$  responsible for the Alfvén effect gets renormalized in strong turbulence ( $B_0(k) \propto k^{-1/3}$ ). When we substitute the renormalized  $B_0$  in Eq. (1.1), the energy spectrum turns out to be proportional to  $k^{-5/3}$ . Sridhar and Goldreich [21], and Goldreich and Sridhar [22] used wave interaction picture and showed that the energy spectrum is anisotropic, and it follows Kolmogorov's powerlaw for strong turbulence.

In this paper we calculate the renormalized viscosity and resistivity for MHD. Here we test whether Kolmogorov's spectrum is a consistent solution of RG or not if the turbulence is forced at large-scale. We carry out wavenumber elimination and obtain recursive RG equations. Kolmogorov's spectrum is substituted for the correlation function in the recursive RG equation. After that we attempt to obtain a convergent solution for the renormalized viscosity and resistivity. If the convergent solution exists, then the Kolmogorov's spectrum is one of the correct choices for the energy spectrum of MHD turbulence. For these cases we compute many important quantities, e.g., renormalized viscosity, renormalized resistivity, cascade rates, etc., in a reasonably simple manner. In this paper we report the calculation of renormalized viscosity and resistivity, and in the subsequent paper (referred to as paper II) we will report the cascade rate calculation.

There are two field variables in MHD: the velocity fluctuation  $\mathbf{u}$  and the magnetic field fluctuation  $\mathbf{b}$ . The quantities of interest are Kinetic energy (KE), magnetic energy (ME), total energy (KE+ME), and cross helicity ( $H_c = \mathbf{u} \cdot \mathbf{b}$ ). The dimensionless parameters used in this paper are the ratio of twice the cross helicity and the total energy, called the normalized cross helicity  $\sigma_c$  ( $\sigma_c = 2H_c/(KE + ME)$ ), and the ratio of KE and ME, called the Alfvén ratio  $r_A$ . In this paper we have assumed that the mean magnetic field is zero, and so are magnetic and kinetic helicities, i.e., we are considering nonhelical plasma. The calculation of the renormalized parameters is quite complex for arbitrary  $\sigma_c$  and  $r_A$ . Therefore, we limit ourselves to two limiting cases: (1)  $\sigma_c = 0$  and whole range of  $r_A$ ; (2)  $\sigma_c \rightarrow 1$  and  $r_A = 1$ . Even though full range of  $\sigma_c$  is observed in terrestrial and extraterrestrial plasmas, the case  $\sigma_c \approx 0$  is most pronounced.

The outline of the paper is as follows: in sections 2 and 3 we compute the renormalized viscosity and resistivity for the cases  $\sigma_c = 0$  and  $\sigma_c \rightarrow 1$  respectively. Section 4 contains the summary and conclusions.

## II. RG CALCULATION: $\sigma_c = 0$

In this section we will calculate the renormalized viscosity and resistivity of MHD equations for zero mean magnetic field and zero cross helicity ( $\sigma_c = 0$ ). In this case, the RG equations in terms of velocity and magnetic field variables are simpler as compared to those with Elsässer variables. Therefore, we will work with  $\mathbf{u}$  and  $\mathbf{b}$  variables. We take the following form of Kolmogorov's spectrum for KE [ $E^u(k)$ ] and ME [ $E^b(k)$ ]

$$E^u(k) = K^u \Pi^{2/3} k^{-5/3}, \quad (2.1)$$

$$E^b(k) = E^u(k)/r_A, \quad (2.2)$$

where  $K^u$  is Kolmogorov's constant for MHD turbulence, and  $\Pi$  is the total energy flux. In the limit  $\sigma_c = 0$ , we have  $E^+ = E^-$  and  $\Pi^+ = \Pi^- = \Pi$  [cf. Eq. (1.3)]. Therefore,  $E_{total}(k) = E^+(k) = E^u(k) + E^b(k)$  and

$$K^+ = K^u(1 + r_A^{-1}) \quad (2.3)$$

With this preliminaries we start our RG calculation. The incompressible MHD equations in the Fourier space are

$$(-i\omega + \nu k^2) u_i(\hat{k}) = -\frac{i}{2} P_{ijm}^+(\mathbf{k}) \int d\hat{p} [u_j(\hat{p}) u_m(\hat{k} - \hat{p}) - b_j(\hat{p}) b_m(\hat{k} - \hat{p})] \quad (2.4)$$

$$(-i\omega + \eta k^2) b_i(\hat{k}) = -i P_{ijm}^-(\mathbf{k}) \int d\hat{p} [u_j(\hat{p}) b_m(\hat{k} - \hat{p})] \quad (2.5)$$

$$k_i u_i(\mathbf{k}) = 0 \quad (2.6)$$

$$k_i b_i(\mathbf{k}) = 0 \quad (2.7)$$

with

$$P_{ijm}^+(\mathbf{k}) = k_j P_{im}(\mathbf{k}) + k_m P_{ij}(\mathbf{k}); \quad (2.8)$$

$$P_{im}(\mathbf{k}) = \delta_{im} - \frac{k_i k_m}{k^2}; \quad (2.9)$$

$$P_{ijm}^-(\mathbf{k}) = k_j \delta_{im} - k_m \delta_{ij}; \quad (2.10)$$

$$\hat{k} = (\mathbf{k}, \omega); \quad (2.11)$$

$$d\hat{p} = d\mathbf{p} d\omega / (2\pi)^{d+1}. \quad (2.12)$$

Here  $\nu$  and  $\eta$  are the viscosity and the resistivity respectively, and  $d$  is the space dimension.

In our RG procedure the wavenumber range  $(k_N, k_0)$  is divided logarithmically into  $N$  shells. The  $n$ th shell is  $(k_n, k_{n-1})$  where  $k_n = h^n k_0$  ( $h < 1$ ). In the following discussion, we carry out the elimination of the first shell  $(k_1, k_0)$  and obtain the modified MHD equations. We then proceed iteratively to eliminate higher shells and get a general expression for the modified MHD equations. The renormalization group procedure is as follows:

1. We divide the spectral space into two parts: 1. the shell  $(k_1, k_0) = k^>$ , which is to be eliminated; 2.  $(k_N, k_1) = k^<$ , set of modes to be retained. Note that  $\nu_0$  and  $\eta_0$  denote the viscosity and resistivity before the elimination of the first shell.
2. We rewrite Eqs. (2.4, 2.5) for  $k^<$  and  $k^>$ . The equations for  $u_i^<(\hat{k})$  and  $b_i^<(\hat{k})$  modes are

$$\begin{aligned} (-i\omega + \Sigma_{(0)}^{uu}(k)) u_i^<(\hat{k}) + \Sigma_{(0)}^{ub}(k) b_i^<(\hat{k}) &= -\frac{i}{2} P_{ijm}^+(\mathbf{k}) \int d\hat{p} ([u_j^<(\hat{p}) u_m^<(\hat{k} - \hat{p})] \\ &\quad + 2[u_j^<(\hat{p}) u_m^>(\hat{k} - \hat{p})] + [u_j^>(\hat{p}) u_m^>(\hat{k} - \hat{p})] \\ &\quad - \text{Similar terms for } b) \end{aligned} \quad (2.13)$$

$$\begin{aligned} (-i\omega + \Sigma_{(0)}^{bb}(k)) b_i^<(\hat{k}) + \Sigma_{(0)}^{bu}(k) u_i^<(\hat{k}) &= -i P_{ijm}^-(\mathbf{k}) \int d\hat{p} ([u_j^<(\hat{p}) b_m^<(\hat{k} - \hat{p})] \\ &\quad + [u_j^<(\hat{p}) b_m^>(\hat{k} - \hat{p})] + [u_j^>(\hat{p}) b_m^<(\hat{k} - \hat{p})] \\ &\quad + [u_j^>(\hat{p}) b_m^>(\hat{k} - \hat{p})]) \end{aligned} \quad (2.14)$$

The  $\Sigma$ s appearing in the equations are usually called the ‘‘self-energy’’ in Quantum field theory language. In the first iteration,  $\Sigma_{(0)}^{uu} = \nu_{(0)} k^2$  and  $\Sigma_{(0)}^{bb} = \eta_{(0)} k^2$ , while the other two  $\Sigma$ s are zero. The equation for  $u_i^>(\hat{k})$  modes can be obtained by interchanging  $<$  and  $>$  in the above equations.

3. The terms given in the second and third brackets in the Right-hand side of Eqs. (2.13, 2.14) are calculated perturbatively. Since we are interested in the statistical properties of  $\mathbf{u}$  and  $\mathbf{b}$  fluctuations, we perform the usual ensemble average of the system [4]. We assume that  $\mathbf{u}^>(\hat{k})$  and  $\mathbf{b}^>(\hat{k})$  have gaussian distributions with zero mean, while  $\mathbf{u}^<(\hat{k})$  and  $\mathbf{b}^<(\hat{k})$  are unaffected by the averaging process. Hence,

$$\langle u_i^>(\hat{k}) \rangle = 0 \quad (2.15)$$

$$\langle b_i^>(\hat{k}) \rangle = 0 \quad (2.16)$$

$$\langle u_i^<(\hat{k}) \rangle = u_i^<(\hat{k}) \quad (2.17)$$

$$\langle b_i^<(\hat{k}) \rangle = b_i^<(\hat{k}) \quad (2.18)$$

and

$$\langle u_i^>(\hat{p})u_j^>(\hat{q}) \rangle = P_{ij}(\mathbf{p})C^{uu}(\hat{p})\delta(\hat{p} + \hat{q}) \quad (2.19)$$

$$\langle b_i^>(\hat{p})b_j^>(\hat{q}) \rangle = P_{ij}(\mathbf{p})C^{bb}(\hat{p})\delta(\hat{p} + \hat{q}) \quad (2.20)$$

$$\langle u_i^>(\hat{p})b_j^>(\hat{q}) \rangle = P_{ij}(\mathbf{p})C^{ub}(\hat{p})\delta(\hat{p} + \hat{q}) \quad (2.21)$$

The triple order correlations  $\langle X_i^>(\hat{k})X_j^>(\hat{p})X_m^>(\hat{q}) \rangle$  are zero due to Gaussian nature of the fluctuations. Here,  $X$  stands for  $u$  or  $b$ . In addition, we also neglect the contribution from the triple nonlinearity  $\langle X_i^<(\hat{k})X_j^<(\hat{p})X_m^<(\hat{q}) \rangle$ . The last assumption is used in many of the turbulence RG calculations [4,5]. Refer to Zhou and Vahala [25] for a discussion on the importance of the triple nonlinearity.

4. The details of the perturbative calculation is given in Appendix A. To the first order, the second bracketed terms of Eqs. (2.13, 2.14) vanish, but the nonvanishing third bracketed terms yield corrections to  $\Sigma$ s. Eqs. (2.13, 2.14) can now be approximated by

$$\begin{aligned} (-i\omega + \Sigma_{(0)}^{uu} + \delta\Sigma_{(0)}^{uu}) u_i^<(\hat{k}) + (\Sigma_{(0)}^{ub} + \delta\Sigma_{(0)}^{ub}) b_i^<(\hat{k}) &= -\frac{i}{2}P_{ijm}^+(\mathbf{k}) \int d\hat{p} [u_j^<(\hat{p})u_m^<(\hat{k} - \hat{p}) \\ &\quad - b_j^<(\hat{p})b_m^<(\hat{k} - \hat{p})] \end{aligned} \quad (2.22)$$

$$\begin{aligned} (-i\omega + \Sigma_{(0)}^{bb} + \delta\Sigma_{(0)}^{bb}) b_i^<(\hat{k}) + (\Sigma_{(0)}^{bu} + \delta\Sigma_{(0)}^{bu}) u_i^<(\hat{k}) &= -iP_{ijm}^-(\mathbf{k}) \int d\hat{p} [u_j^<(\hat{p})b_m^<(\hat{k} - \hat{p})] \end{aligned} \quad (2.23)$$

with

$$\begin{aligned} \delta\Sigma_{(0)}^{uu}(k) &= \frac{1}{(d-1)k^2} \int_{\hat{p}+\hat{q}=\hat{k}}^{\Delta} d\hat{p} [S(k, p, q)G^{uu}(\hat{p})C^{uu}(\hat{q}) - S_6(k, p, q)G^{bb}(\hat{p})C^{bb}(\hat{q}) \\ &\quad + S_6(k, p, q)G^{ub}(\hat{p})C^{ub}(\hat{q}) - S(k, p, q)G^{bu}(\hat{p})C^{ub}(\hat{q})] \end{aligned} \quad (2.24)$$

$$\begin{aligned} \delta\Sigma_{(0)}^{ub}(k) &= \frac{1}{(d-1)k^2} \int_{\hat{p}+\hat{q}=\hat{k}}^{\Delta} d\hat{p} [-S(k, p, q)G^{uu}(\hat{p})C^{ub}(\hat{q}) + S_5(k, p, q)G^{ub}(\hat{p})C^{uu}(\hat{q}) \\ &\quad + S(k, p, q)G^{bu}(\hat{p})C^{bb}(\hat{q}) - S_5(k, p, q)G^{bb}(\hat{p})C^{ub}(\hat{q})] \end{aligned} \quad (2.25)$$

$$\begin{aligned} \delta\Sigma_{(0)}^{bu}(k) &= \frac{1}{(d-1)k^2} \int_{\hat{p}+\hat{q}=\hat{k}}^{\Delta} d\hat{p} [S_8(k, p, q)G^{uu}(\hat{p})C^{ub}(\hat{q}) + S_{10}(k, p, q)G^{bb}(\hat{p})C^{ub}(\hat{q}) \\ &\quad + S_{12}(k, p, q)G^{ub}(\hat{p})C^{bb}(\hat{q}) - S_7(k, p, q)G^{bu}(\hat{p})C^{uu}(\hat{q})] \end{aligned} \quad (2.26)$$

$$\begin{aligned} \delta\Sigma_{(0)}^{bb}(k) &= \frac{1}{(d-1)k^2} \int_{\hat{p}+\hat{q}=\hat{k}}^{\Delta} d\hat{p} [-S_8(k, p, q)G^{uu}(\hat{p})C^{bb}(\hat{q}) + S_9(k, p, q)G^{bb}(\hat{p})C^{uu}(\hat{q}) \\ &\quad + S_{11}(k, p, q)G^{ub}(\hat{p})C^{ub}(\hat{q}) - S_9(k, p, q)G^{bu}(\hat{p})C^{ub}(\hat{q})] \end{aligned} \quad (2.27)$$

The quantities  $S_i(k, p, q)$  are given in the Appendix B. The integral  $\Delta$  is to be done over the first shell.

The full-fledge calculation of  $\Sigma$ s is quite involved. Therefore, we take two special cases: (1)  $C^{ub} = 0$  or  $\sigma_c = 0$ ; and (2)  $C^{ub} \approx C^{uu} \approx C^{bb}$  or  $\sigma_c \rightarrow 1$ . In this section we will discuss only the case  $\sigma_c = 0$ . The other case will be taken up in the next section. A word of caution is in order here. In our calculation the parameters used are  $\sigma_c(k) = 2C^{ub}(k)/(C^{uu}(k) + C^{bb}(k))$  and  $r_A(k) = E^u(k)/E^b(k)$ . These parameters differ from the global  $\sigma_c$  and  $r_A$ , yet we have restricted ourselves to the limiting cases of constant  $\sigma_c(k)$  and  $r_A(k)$  because of simplicity.

When  $\sigma_c = 0$ , an inspection of the self-energy diagrams shows that  $\Sigma^{ub} = \Sigma^{bu} = 0$ , and  $G^{ub} = G^{bu} = 0$ . Clearly, the equations become much simpler because of the diagonal nature of matrices  $G$  and  $\Sigma$ . The two quantities of interest  $\delta\Sigma_{(0)}^{uu}$  and  $\delta\Sigma_{(0)}^{bb}$  will be given by

$$\delta\Sigma_{(0)}^{uu}(\hat{k}) = \frac{1}{d-1} \int_{\hat{p}+\hat{q}=\hat{k}}^{\Delta} d\hat{p} (S(k, p, q)G^{uu}(p)C^{uu}(q) - S_6(k, p, q)G^{bb}(p)C^{bb}(q)) \quad (2.28)$$

$$\delta\Sigma_{(0)}^{bb}(\hat{k}) = \frac{1}{d-1} \int_{\hat{p}+\hat{q}=\hat{k}}^{\Delta} d\hat{p} (-S_8(k, p, q)G^{uu}(p)C^{bb}(q) + S_9(k, p, q)G^{bb}(p)C^{uu}(q)) \quad (2.29)$$

The expressions for  $\delta\Sigma$ 's involves correlation functions and Green's function, which are themselves functions of  $\Sigma$ 's. In earlier RG calculations (see e.g. [1,4]) the correlation function  $C(\vec{k})$  is function of forcing noise spectrum. In our self-consistent scheme we assume that we are in the inertial range, and the energy spectrum is proportional to Kolmogorov's 5/3 powerlaw. After that the renormalized Green's function, or renormalized  $\nu$  is computed iteratively.

The frequency dependence of the correlation function are taken as:  $C^{uu}(k, \omega) = 2C^{uu}(k)\Re(G^{uu}(k, \omega))$  and  $C^{bb}(k, \omega) = 2C^{bb}(k)\Re(G^{bb}(k, \omega))$ . In other words, the relaxation time-scale of correlation function is assumed to be the same as that of corresponding Green's function. Since we are interested in large time-scale behaviour of turbulence, we take the limit  $\omega$  going to zero. Under these assumptions, the above equations become

$$\delta\nu_{(0)}(k) = \frac{1}{(d-1)k^2} \int_{\mathbf{p}+\mathbf{q}=\mathbf{k}}^{\Delta} \frac{d\mathbf{p}}{(2\pi)^d} \left[ S(k, p, q) \frac{C^{uu}(q)}{\nu_{(0)}(p)p^2 + \nu_{(0)}(q)q^2} - S_6(k, p, q) \frac{C^{bb}(q)}{\eta_{(0)}(p)p^2 + \eta_{(0)}(q)q^2} \right] \quad (2.30)$$

$$\delta\eta_{(0)}(k) = \frac{1}{(d-1)k^2} \int_{\mathbf{p}+\mathbf{q}=\mathbf{k}}^{\Delta} \frac{d\mathbf{p}}{(2\pi)^d} \left[ -S_9(k, p, q) \frac{C^{bb}(q)}{\nu_{(0)}(p)p^2 + \eta_{(0)}(q)q^2} + S_9(k, p, q) \frac{C^{uu}(q)}{\eta_{(0)}(p)p^2 + \nu_{(0)}(q)q^2} \right] \quad (2.31)$$

Note that  $\nu(k) = \Sigma^{uu}(k)/k^2$  and  $\eta(k) = \Sigma^{bb}(k)/k^2$ .

There are some important points to remember in the above step. The frequency integral in the above is done using contour integral. It can be shown that the integrals are nonzero only when both the components appearing the denominator are of the same sign. For example, first term of Eq. (2.31) is nonzero only when both  $\nu_{(0)}(p)$  and  $\eta_{(0)}(q)$  are of the same sign.

Let us denote  $\nu_{(1)}(k)$  and  $\eta_{(1)}(k)$  as the renormalized viscosity and resistivity respectively after the first step of wavenumber elimination. Hence,

$$\nu_{(1)}(k) = \nu_{(0)}(k) + \delta\nu_{(0)}(k); \quad (2.32)$$

$$\eta_{(1)}(k) = \eta_{(0)}(k) + \delta\eta_{(0)}(k) \quad (2.33)$$

5. We keep eliminating the shells one after the other by the above procedure. After  $n+1$  iterations we obtain

$$\nu_{(n+1)}(k) = \nu_{(n)}(k) + \delta\nu_{(n)}(k) \quad (2.34)$$

$$\eta_{(n+1)}(k) = \eta_{(n)}(k) + \delta\eta_{(n)}(k) \quad (2.35)$$

where the equations for  $\delta\nu_{(n)}(k)$  and  $\delta\eta_{(n)}(k)$  are the same as the Eqs. (2.30, 2.31) except that  $\nu_{(0)}(k)$  and  $\eta_{(0)}(k)$  appearing in the equations are to be replaced by  $\nu_{(n)}(k)$  and  $\eta_{(n)}(k)$  respectively. Clearly  $\nu_{(n+1)}(k)$  and  $\eta_{(n+1)}(k)$  are the renormalized viscosity and resistivity after the elimination of the  $(n+1)$ th shell.

6. We need to compute  $\delta\nu_{(n)}$  and  $\delta\eta_{(n)}$  for various  $n$ . These computations, however, require  $\nu_{(n)}$  and  $\eta_{(n)}$ . In our scheme we solve these equations iteratively. In Eqs. (2.30, 2.31) we substitute  $C(k)$  by one dimensional energy spectrum  $E(k)$

$$C^{uu}(k) = \frac{2(2\pi)^d}{S_d(d-1)} k^{-(d-1)} E^u(k) \quad (2.36)$$

$$C^{bb}(k) = \frac{2(2\pi)^d}{S_d(d-1)} k^{-(d-1)} E^b(k) \quad (2.37)$$

where  $S_d$  is the surface area of  $d$  dimensional spheres. We assume that  $E^u(k)$  and  $E^b(k)$  follow Eqs. (2.1, 2.2) respectively. Regarding  $\nu_{(n)}$  and  $\eta_{(n)}$ , we attempt the following form of solution

$$\nu_{(n)}(k_n k') = (K^u)^{1/2} \Pi^{1/3} k_n^{-4/3} \nu_{(n)}^*(k') \quad (2.38)$$

$$\eta_{(n)}(k_n k') = (K^u)^{1/2} \Pi^{1/3} k_n^{-4/3} \eta_{(n)}^*(k') \quad (2.39)$$

with  $k = k_{n+1}k'(k' < 1)$ . We expect  $\nu_{(n)}^*(k')$  and  $\eta_{(n)}^*(k')$  to be universal functions for large  $n$ . The substitution of  $C^{uu}(k), C^{bb}(k), \nu_{(n)}(k)$ , and  $\eta_{(n)}(k)$  yields the following equations:

$$\delta\nu_{(n)}^*(k') = \frac{1}{(d-1)} \int_{\mathbf{p}'+\mathbf{q}'=\mathbf{k}'} d\mathbf{q}' \frac{2}{(d-1)S_d} \frac{E^u(q')}{q'^{d-1}} \times \left[ S(k', p', q') \frac{1}{\nu_{(n)}^*(hp')p'^2 + \nu_{(n)}^*(hq')q'^2} - S_6(k', p', q') \frac{r_A^{-1}}{\eta_{(n)}^*(hp')p'^2 + \eta_{(n)}^*(hq')q'^2} \right] \quad (2.40)$$

$$\delta\eta_{(n)}^*(k') = \frac{1}{(d-1)} \int_{\mathbf{p}'+\mathbf{q}'=\mathbf{k}'} d\mathbf{q}' \frac{2}{(d-1)S_d} \frac{E^u(q')}{q'^{d-1}} \times \left[ -S_8(k', p', q') \frac{1}{\nu_{(n)}^*(hp')p'^2 + \eta_{(n)}^*(hq')q'^2} + S_9(k', p', q') \frac{r_A^{-1}}{\eta_{(n)}^*(hp')p'^2 + \nu_{(n)}^*(hq')q'^2} \right] \quad (2.41)$$

$$\nu_{(n+1)}^*(k') = h^{4/3}\nu_{(n)}^*(hk') + h^{-4/3}\delta\nu_{(n)}^*(k') \quad (2.42)$$

$$\eta_{(n+1)}^*(k') = h^{4/3}\eta_{(n)}^*(hk') + h^{-4/3}\delta\eta_{(n)}^*(k') \quad (2.43)$$

where the integrals in the above equations are performed iteratively over a region  $1 \leq p', q' \leq 1/h$  with the constraint that  $\mathbf{p}' + \mathbf{q}' = \mathbf{k}'$ . Fournier and Frisch [3] showed the above volume integral in  $d$  dimension to be

$$\int_{\mathbf{p}'+\mathbf{q}'=\mathbf{k}'} d\mathbf{q}' = S_{d-1} \int dpdq \left(\frac{pq}{k}\right)^{d-2} (\sin \alpha)^{d-3} \quad (2.44)$$

where  $\alpha$  is the angle between vectors  $\mathbf{p}$  and  $\mathbf{q}$ .

- Now we solve the above four equations self consistently for various  $r_A$ s. We have taken  $h = 0.7$ . We start with constant values of  $\nu_{(0)}^*$  and  $\eta_{(0)}^*$  and compute the integrals using Gauss quadrature technique. Once  $\delta\nu_{(0)}^*$  and  $\delta\eta_{(0)}^*$  have been computed, we can calculate  $\nu_{(1)}^*$  and  $\eta_{(1)}^*$ . We iterate this process till  $\nu_{(m+1)}^*(k') \approx \nu_{(m)}^*(k')$  and  $\eta_{(m+1)}^*(k') \approx \eta_{(m)}^*(k')$ , that is, till they converge. We have reported the limiting  $\nu^*$  and  $\eta^*$  whenever the solution converges. The criterion for convergence is that the error must be less than 1%. This criterion is usually achieved by  $n = 10$  or so. The result of our RG analysis is given below.

We have carried out the RG analysis for various space dimensions and find that the solution converges for all  $d > d_c \approx 2.2$ . Hence, the RG fixed-point for MHD turbulence is stable for  $d \geq d_c$ . For illustration of convergent solution, see Fig. 1 for the plots of  $\nu_{(n)}^*(k')$  and  $\eta_{(n)}^*(k')$  for  $d = 3, r_A = 1$ . The RG fixed point for  $d < d_c$  is unstable. Refer to the plots of Fig. 2 for  $d = 2, r_A = 1$  as an example of an unstable solution. From this observation we can claim that Kolmogorov's powerlaw is a consistent solution of MHD RG equations at least for  $d \geq d_c$ . The values of asymptotic ( $k' \rightarrow 0$  limit)  $\nu^*$  and  $\eta^*$  for various  $d$  and  $r_A = 1$  are displayed in Table I. Clearly  $\nu^*$  and  $\eta^*$  decreases with the increase in  $d$  for  $d \geq 4$ . The plot of Fig. (3) shows that both  $\nu^*$  and  $\eta^*$  are proportional to  $d^{-1/2}$ . In the same plot we have also displayed  $\nu^*$  for pure fluid turbulence; there too  $\nu^* \propto d^{-1/2}$ . This result is consistent with Fournier *et al.*'s prediction for fluid turbulence [23].

An important point to note is that the stability of RG fixed point in a given space dimension depends on Alfvén ratio and normalized cross helicity. For example, for  $d = 2.2$  the RG fixed point is stable for  $r_A \geq 1$ , but unstable for  $r_A < 1$ . A detailed study of stability of the RG fixed point is required to ascertain the boundary of stability.

The values of renormalized parameters for  $d = 3$  and various  $r_A$  are shown in Table II. For large  $r_A$  (fluid dominated regime),  $\nu^*$  is close to renormalized viscosity of fluid turbulence ( $r_A = \infty$ ), but  $\eta^*$  is also finite. That means there is a positive magnetic energy flux even when  $r_A \rightarrow \infty$ . As  $r_A$  is decreased,  $\eta^*$  decreases but  $\nu^*$  increases, or the Prandtl number  $Pr = \nu/\eta$  increases. This trend is seen till  $r_A \approx 0.25$  where the RG fixed point with nonzero  $\nu^*$  and  $\eta^*$  becomes unstable, and the trivial RG fixed point with  $\nu^* = \eta^* = 0$  becomes stable. This result suggests an absence of turbulence for  $r_A$  below 0.25 (approximately). Note that in the  $r_A \rightarrow 0$  (fully magnetic) limit, the MHD equations become linear, hence there is no turbulence. Surprisingly, our RG calculation suggests that turbulence disappear near  $r_A = 0.25$  itself.

The final  $\nu^*(k')$  and  $\eta^*(k')$  are constant for small  $k'$  but shifts towards zero for larger  $k'$  (see Fig. 1). Similar behaviour has been seen by McComb and coworkers [24] for fluid turbulence; this behaviour is attributed to the neglect of triple nonlinearity, and the corrective procedure has been prescribed by Zhou and Vahala [25]. For simplicity we have not included the effects of triple nonlinearity in our calculation.

Kraichnan's  $k^{-3/2}$  energy spectrum [see Eq. (1.1)] and  $\sigma^{uu} = \sigma^{bb} \propto kB_0$  do not satisfy the RG equations. This implies that Kraichnan's  $3/2$  powerlaw is not a consistent solution of RG equations.

Pouquet [26] and Ishizawa and Hattori [27] calculated the contributions to the renormalized (eddy) viscosity and resistivity from each of the four nonlinear terms of MHD equations using EDQNM (Eddy-Damped-Quasi-Normal-Markovian) approximation. This calculation has been done for  $d = 2$ . Let us denote the quantities  $\nu^{uu}$ ,  $\nu^{ub}$ ,  $\eta^{bu}$ ,  $\eta^{bb}$  as contributions from the terms  $\mathbf{u} \cdot \nabla \mathbf{u}$ ,  $-\mathbf{b} \cdot \nabla \mathbf{b}$ ,  $-\mathbf{u} \cdot \nabla \mathbf{b}$ ,  $\mathbf{b} \cdot \nabla \mathbf{u}$  respectively. Note that various cascade rates of MHD turbulence [27–29] can be inferred from these parameters. The cascade rate from inside of the  $X$  sphere ( $X <$ ) to outside of the  $Y$  sphere ( $Y >$ ) is

$$\Pi_{Y>}^{X<} = \int_0^{k_N} 2\nu^{XY}(k)k^2 E^X(k)dk \quad (2.45)$$

where  $X, Y$  denote  $u$  or  $b$ . We have computed  $\nu^{XY}$  for  $d \geq d_c$ ; their values are listed in Tables I and II. Our results show that  $\eta^{bb}$  is positive. Pouquet argues that  $\eta^{bb}$  is negative, while Ishizawa finds it to be positive. Since our RG procedure is applicable only for  $d > d_c = 2.2$ , it is not proper to compare our results with those of Pouquet [26] and Ishizawa and Hattori [27]. However, we can claim that the magnetic energy cascade rate ( $\Pi_{b>}^{b<}$ ) is positive for all  $d > d_c$  because  $\eta^{bb} > 0$ .

The eddy viscosity and resistivity listed in Table I shows that  $\eta^{bb*}$  and  $\nu^{ub*}$  decrease as  $d$  increases. On the contrary,  $\eta^{bu*}$  and  $\nu^{uu*}$  first increases till around  $d = 5$  then decreases as  $d$  increases. Since MHD fluxes are proportional to these parameters, the corresponding fluxes decrease as  $d$  is increased beyond 5. Near  $d = 2$ ,  $\nu^{uu*}$  is negative, reminiscent of inverse cascade energy in two-dimensional fluid turbulence in the  $5/3$  region. Also,  $\eta^{bu*}$  is negative near  $d = 2$ , i.e., there is a negative energy cascade from  $b$ -sphere to outside  $u$ -sphere. The above results are consistent with the recent simulation results of Dar *et al.* [29] on two-dimensional MHD turbulence.

The variation of  $\nu^{XY*}$  with  $r_A$  for  $d = 3$  is displayed in Tables II. For large  $r_A$ ,  $\nu^{uu*}$  is close to the fluid turbulence  $\nu^*$ . However,  $\eta^{bb*}$  also finite. Hence there is a significant magnetic energy cascade from  $b$ -sphere to outside  $b$ -sphere even in fluid dominated case. As  $r_A$  is decreased,  $\nu^{ub*}$  and  $\eta^{bu*}$  increase, hence cascade rates from  $u$ -sphere to outside  $b$ -sphere, and  $b$ -sphere to outside  $u$ -sphere start becoming important. Incidentally, both  $\nu^{uu*}$  and  $\eta^{bb*}$  decrease as  $r_A$  decreases.

In this section we have calculated the renormalized viscosity and resistivity for  $\sigma_c = 0$ . In the next section we will calculate these parameters for the  $\sigma_c \rightarrow 1$  limit.

### III. RG CALCULATION: $\sigma_c \rightarrow 1$

The  $\mathbf{u}$  and  $\mathbf{b}$  correlation is very high when  $\sigma_c \rightarrow 1$ . For this case it is best to work with Elsässer variables  $\mathbf{z}^\pm = \mathbf{u} \pm \mathbf{b}$ . In terms of Elsässer variables,  $\langle |z^+|^2 \rangle \gg \langle |z^-|^2 \rangle$ . These types of fluctuations have been observed in the solar wind near the Sun. However, by the time the solar wind approaches Earth, the normalized cross helicity is close to zero.

In this section we will briefly discuss the RG treatment for the above case. For the following discussion we will denote  $\langle |z^-|^2 \rangle / \langle |z^+|^2 \rangle = r = (1 - \sigma_c) / (1 + \sigma_c)$ . Clearly  $r \ll 1$ .

MHD equations in terms of Elsässer variables are

$$(-i\omega + \nu_{(0)\pm\pm}k^2) z_i^\pm(\hat{k}) + \nu_{(0)\pm\mp}k^2 z_i^\mp(\hat{k}) = -iM_{ijm}(\mathbf{k}) \int d\hat{p} [z_j^\mp(\hat{p})z_m^\pm(\hat{k} - \hat{p})] \quad (3.1)$$

where

$$M_{ijm}(\mathbf{k}) = k_j P_{im}(\mathbf{k}) \quad (3.2)$$

Note that the above equations contain four dissipative coefficients  $\nu_{\pm\pm}$  and  $\nu_{\pm\mp}$  instead of usual two constants  $\nu_\pm = (\nu \pm \eta)/2$ . This is because  $+-$  symmetry is broken in this case, consequently RG generates the other two constants. We carry out the same procedure as outlined in the previous section. After  $n + 1$  steps of the RG calculation, the above equations become

$$\begin{aligned} & [-i\omega \mp (\nu_{(n)\pm\pm}(k) + \delta\nu_{(n)\pm\pm}(k)) k^2] z_i^{\pm<}(\hat{k}) \\ & + (\nu_{(n)\pm\mp}(k) + \delta\nu_{(n)\pm\mp}(k)) k^2 z_i^{\mp<}(\hat{k}) = -iM_{ijm}(\mathbf{k}) \int d\hat{p} z_j^{\mp<}(\hat{p}) z_m^{\pm<}(\hat{k} - \hat{p}) \end{aligned} \quad (3.3)$$

with

$$\delta\nu_{(n)++}(k) = \frac{1}{(d-1)k^2} \int_{\hat{p}+\hat{q}=\hat{k}}^{\Delta} d\hat{p} [S_1(k, p, q)G_{(n)}^{++}(\hat{p})C^{--}(\hat{q}) + S_2(k, p, q)G_{(n)}^{+-}(\hat{p})C^{--}(\hat{q}) \\ + S_3(k, p, q)G_{(n)}^{-+}(\hat{p})C^{+-}(\hat{q}) + S_4(k, p, q)G_{(n)}^{--}(\hat{p})C^{+-}(\hat{q})] \quad (3.4)$$

$$\delta\nu_{(n)+-}(k) = \frac{1}{(d-1)k^2} \int_{\hat{p}+\hat{q}=\hat{k}}^{\Delta} d\hat{p} [S_1(k, p, q)G_{(n)}^{+-}(\hat{p})C^{-+}(\hat{q}) + S_2(k, p, q)G_{(n)}^{++}(\hat{p})C^{-+}(\hat{q}) \\ + S_3(k, p, q)G_{(n)}^{--}(\hat{p})C^{++}(\hat{q}) + S_4(k, p, q)G_{(n)}^{-+}(\hat{p})C^{++}(\hat{q})] \quad (3.5)$$

where the integral is performed over the  $(n+1)$ th shell  $(k_{n+1}, k_n)$ . The equations for the other two  $\delta\nu$ s can be obtained by interchanging  $+$  and  $-$  signs. Now we assume that the Alfvén ratio is one, i.e.,  $C^{+-} = E^u - E^b = 0$ . Under this condition, the above equations reduce to

$$\delta\nu_{(n)++}(k) = \frac{1}{(d-1)k^2} \int_{\hat{p}+\hat{q}=\hat{k}}^{\Delta} d\hat{p} [S_1(k, p, q)G_{(n)}^{++}(\hat{p}) + S_2(k, p, q)G_{(n)}^{+-}(\hat{p})]C^{--}(\hat{q}) \quad (3.6)$$

$$\delta\nu_{(n)+-}(k) = \frac{1}{(d-1)k^2} \int_{\hat{p}+\hat{q}=\hat{k}}^{\Delta} d\hat{p} [S_3(k, p, q)G_{(n)}^{--}(\hat{p}) + S_4(k, p, q)G_{(n)}^{-+}(\hat{p})]C^{++}(\hat{q}) \quad (3.7)$$

$$\delta\nu_{(n)-+}(k) = \frac{1}{(d-1)k^2} \int_{\hat{p}+\hat{q}=\hat{k}}^{\Delta} d\hat{p} [S_3(k, p, q)G_{(n)}^{++}(\hat{p}) + S_4(k, p, q)G_{(n)}^{+-}(\hat{p})]C^{--}(\hat{q}) \quad (3.8)$$

$$\delta\nu_{(n)--}(k) = \frac{1}{(d-1)k^2} \int_{\hat{p}+\hat{q}=\hat{k}}^{\Delta} d\hat{p} [S_1(k, p, q)G_{(n)}^{--}(\hat{p}) + S_2(k, p, q)G_{(n)}^{-+}(\hat{p})]C^{++}(\hat{q}) \quad (3.9)$$

The inspection of Eqs. (3.6–3.9) reveal that  $\nu_{++}$  and  $\nu_{-+}$  are of the order of  $r$ . Hence, we take the  $\hat{\nu}$  matrix to be of the form

$$\hat{\nu}(k, \omega) = \begin{pmatrix} r\zeta & \alpha \\ r\psi & \beta \end{pmatrix} \quad (3.10)$$

It is convenient to transform the frequency integrals in Eqs. [(3.6–3.9)] into temporal integrals, which leads

$$\delta\nu_{(n)++}(k) = \frac{1}{(d-1)k^2} \int_{\mathbf{p}+\mathbf{q}=\mathbf{k}}^{\Delta} \frac{d\mathbf{p}}{(2\pi)^d} \int_{-\infty}^t dt' [S_1(k, p, q)G_{(n)}^{++}(\mathbf{p}, t-t') + S_2(k, p, q)G_{(n)}^{+-}(\mathbf{p}, t-t')] \\ C^{--}(\mathbf{q}, t-t') \quad (3.11)$$

and similar forms for equations for other  $\nu$ s. Green's function  $\hat{G}(k, t-t') = \exp[-\hat{\nu}k^2(t-t')]$  can be easily evaluated by diagonalizing the matrix  $\hat{\nu}$ . The final form of  $\hat{G}(k, t-t')$  to leading order in  $r$  is

$$\hat{G}(k, t-t') = \begin{pmatrix} 1 - \frac{r\alpha\psi}{\beta^2}(1 - e^{-\beta(t-t')}) & -\left\{ \frac{\alpha}{\beta} + \frac{r\alpha}{\beta} \left( \frac{\zeta}{\beta} - \frac{2\alpha\psi}{\beta^2} \right) \right\} (1 - e^{-\beta(t-t')}) \\ -\frac{r\psi}{\beta}(1 - e^{-\beta(t-t')}) & e^{-\beta(t-t')} + \frac{r\alpha\psi}{\beta^2}(1 - e^{-\beta(t-t')}) \end{pmatrix} \quad (3.12)$$

The correlation matrix  $\hat{C}(k, t-t')$  is given by

$$\begin{pmatrix} C^{++}(k, t-t') & C^{+-}(k, t-t') \\ C^{-+}(k, t-t') & C^{--}(k, t-t') \end{pmatrix} = \hat{G}(k, t-t') \begin{pmatrix} C^{++}(k) & C^{+-}(k) \\ C^{-+}(k) & C^{--}(k) \end{pmatrix} \quad (3.13)$$

The substitution of correlation functions and Green's functions yield the following expressions for the elements of  $\delta\hat{\nu}$

$$\delta\zeta_{(n)}(k) = \frac{1}{(d-1)k^2} \int^{\Delta} \frac{d\mathbf{p}}{(2\pi)^d} C^+(q) \left\{ S_1(k, p, q) \frac{1}{\beta_{(n)}(q)q^2} \right. \\ \left. + S_2(k, p, q) \frac{\alpha_{(n)}(p)}{\beta_{(n)}(p)} \left( \frac{1}{\beta_{(n)}(p)p^2 + \beta_{(n)}(q)q^2} - \frac{1}{\beta_{(n)}(q)q^2} \right) \right. \\ \left. - S_3(k, p, q) \frac{\alpha_{(n)}(q)}{\beta_{(n)}(q)} \left( \frac{1}{\beta_{(n)}(p)p^2 + \beta_{(n)}(q)q^2} - \frac{1}{\beta_{(n)}(p)p^2} \right) \right\} \quad (3.14)$$

$$\delta\alpha_{(n)}(k) = \frac{1}{(d-1)k^2} \int^{\Delta} \frac{d\mathbf{p}}{(2\pi)^d} S_3(k, p, q) \frac{C^+(q)}{\beta_{(n)}(p)p^2} \quad (3.15)$$



$$\begin{aligned} \delta\psi_{(n)}(k) = & \frac{1}{(d-1)k^2} \int^{\Delta} \frac{d\mathbf{p}}{(2\pi)^d} C^+(q) \{ S_3(k, p, q) \frac{1}{\beta_{(n)}(q)q^2} \\ & + S_2(k, p, q) \frac{\alpha_{(n)}(q)}{\beta_{(n)}(q)} \left( \frac{1}{\beta_{(n)}(p)p^2 + \beta_{(n)}(q)q^2} - \frac{1}{\beta_{(n)}(p)p^2} \right) \\ & + S_4(k, p, q) \frac{\alpha_{(n)}(p)}{\beta_{(n)}(p)} \frac{1}{\beta_{(n)}(q)q^2} \} \end{aligned} \quad (3.16)$$

$$\delta\beta_{(n)}(k) = \frac{1}{(d-1)k^2} \int^{\Delta} \frac{d\mathbf{p}}{(2\pi)^d} S_1(k, p, q) \frac{C^+(q)}{\beta_{(n)}(p)p^2} \quad (3.17)$$

Note that  $\delta\alpha$ ,  $\delta\beta$ ,  $\delta\zeta$ ,  $\delta\psi$ , and hence  $\alpha$ ,  $\beta$ ,  $\zeta$ ,  $\psi$ , are all independent of  $r$ . To solve the above equations we substitute the following one-dimensional energy spectra in the above equations:

$$E^+(k) = K^+ \frac{(\Pi^+)^{4/3}}{(\Pi^-)^{2/3}} k^{-5/3} \quad (3.18)$$

$$E^-(k) = rE^+(k), \quad (3.19)$$

For the elements of  $\hat{\nu}$  we substitute

$$Z_{(n)}(k) = Z_{(n)}^* \sqrt{K^+} \frac{(\Pi^+)^{2/3}}{(\Pi^-)^{1/3}} k^{-4/3} \quad (3.20)$$

where  $Z$  stands for  $\zeta, \alpha, \psi, \beta$ . The renormalized  $Z^*$ s are calculated using the procedure outlined in the previous section. For large  $n$  their values for  $d = 3$  are

$$\hat{Z}^* = \begin{pmatrix} 0.86r & 0.14 \\ 0.16r & 0.84 \end{pmatrix}, \quad (3.21)$$

and for  $d = 2$  they are

$$\hat{Z}^* = \begin{pmatrix} 0.95r & 0.54 \\ 1.10r & 0.54 \end{pmatrix} \quad (3.22)$$

Note that the solution converges for both  $d = 2$  and  $d = 3$ .

As discussed in the earlier section, the cascade rates  $\Pi^{\pm}$  can be calculated from the renormalized parameters discussed above. Using the energy equations we can easily derive the equations for the cascade rates, which are

$$\Pi^+ = \int_0^{k_N} 2r\zeta k^2 E^+(k) + \int_0^{k_N} 2\alpha k^2 (E^u(k) - E^b(k)) \quad (3.23)$$

$$\Pi^- = \int_0^{k_N} 2\beta k^2 E^-(k) + \int_0^{k_N} 2r\psi k^2 (E^u(k) - E^b(k)) \quad (3.24)$$

Under the assumption that  $r_A = 1$ , the parts of  $\Pi^{\pm}$  proportional to  $(E^u(k) - E^b(k))$  vanish. Hence, the total cascade rate will be

$$\Pi = \frac{1}{2}(\Pi^+ + \Pi^-) \quad (3.25)$$

$$= r \int_0^{k_N} (\zeta + \beta) k^2 E^+(k) \quad (3.26)$$

Since  $\zeta$  and  $\beta$  are independent of  $r$ , the total cascade rate is proportional to  $r$  (for  $r$  small). Clearly the cascade rate  $\Pi$  vanishes when  $r = 0$  or  $\sigma_c = 1$ . This result is consistent with the fact that the nonlinear interactions are absent when only pure Alfvén waves ( $z^+$  or  $z^-$ ) are present. The detailed calculation of the cascade rates  $\Pi^{\pm}$  and the constants  $K^{\pm}$  is left for future studies (paper II).

#### IV. SUMMARY AND CONCLUSIONS

In this paper we have constructed a self-consistent RG scheme for MHD turbulence and computed the renormalized viscosity and resistivity. These quantities find applications in simulations specially large-eddy-simulations (LES). In our RG scheme we assume that we are in the fully nonlinear range, and the renormalized energy spectrum is substituted for the correlation function. After the substitution of the correlation function, the renormalized Greens function or renormalized viscosity and resistivity are computed iteratively. In our procedure Kolmogorov's powerlaw is taken for the energy spectrum, and it is shown to be a self-consistent solution of the RG equation for  $d \geq d_c \approx 2.2$ . This result is consistent with the recent theoretical [10,21,22], numerical [18–20], and observational studies of solar wind [16,17] that favor Kolmogorov's spectrum for MHD turbulence. Note that we do not carry out vertex (the coefficient of the nonlinear term) renormalization; there is an implicit assumption that the vertex renormalization, if any, is included when we substitute renormalized energy spectrum (Kolmogorov's) in the RG equation.

For simplicity of the calculation we have taken two special cases: (1)  $\sigma_c = 0$  and full range of  $r_A$ ; (2)  $\sigma_c \rightarrow 1$  and  $r_A = 1$ . For these two cases, the renormalized viscosity and resistivity have been calculated for various space dimensions. For  $\sigma_c = 0$ , there exists a stable RG fixed point for  $d \geq d_c \approx 2.2$ . The RG fixed point is unstable for  $d < d_c$ . Our result is consistent with that Liang and Diamond [9] where they conclude that the RG fixed point for  $d = 2$  is unstable. Note however that the stability depends on the value of  $r_A$  and  $\sigma_c$ . An exhaustive study is required to ascertain the boundary of stability as a function of  $d, \sigma_c$ , and  $r_A$ .

Some interesting trends emerge as we vary space dimensionality. For  $r_A = 1$ , the parameters  $\nu^{ub*}$  and  $\eta^{bb*}$  decrease with the increase of  $d$ , but  $\nu^{uu*}$  and  $\eta^{bu*}$  first increase till  $d \approx 5$  then decrease.

For  $d = 3$ , variation of  $r_A$  shows some interesting features. For large  $r_A$ ,  $\nu^*$  is close to the  $\nu^*$  for pure fluid turbulence, but  $\eta^*$  is also finite for this case. As  $r_A$  is decreased,  $\nu^*$  increases and  $\eta^*$  decreases, or  $Pr = \nu/\eta$  increases. Another important result of our calculation is absence of turbulence for all  $r_A$  below 0.25 or so. In the  $r_A \rightarrow 0$  (fully magnetic) limit, the MHD equations become linear, hence there is no turbulence. It is however surprising that turbulence disappears near  $r_A = 0.25$  itself.

Our RG calculation for fluid turbulence ( $r_A = \infty$ ) show several interesting features. The RG fixed point is stable for  $d = 2$ , and the renormalized viscosity is approximately  $-0.5$ , a *negative* number. This is consistent with the inverse cascade of energy for the 5/3 region. Note however that for  $d = 3$ , the renormalized fluid viscosity is positive (0.38), hence the energy cascade is forward, consistent with Kolmogorov's hypothesis.

The values of the renormalized viscosity and resistivity calculated by our calculation differs from that of Verma and Bhattacharjee [30], the later calculation being similar to Kraichnan's Direct-Interaction-Approximation calculation for fluid turbulence. Verma and Bhattacharjee [30] assumed  $\nu^{++} = \nu^{-+}$  and  $\nu^{+-} = \nu^{--}$ , which is correct only in a limited region of parameter space. In addition, they assumed a cutoff for the self-energy calculation to cure infrared divergence. In the present calculation we have overcome both these defects, and expect that the numbers reported here will match with the future simulation results. It is unfortunate that the RG scheme fails for  $d = 2$ , hence, several numerical results of 2D-MHD turbulence [18–20,29] could not be compared with the analytic results presented here.

Kraichnan's 3/2 energy spectrum and  $\Sigma^{uu} = \Sigma^{bb} \propto (kB_0)$  do not satisfy renormalization group equations [Eqs. (2.30–2.33)]. Hence  $E(k) \propto k^{-3/2}$  is not a consistent solution of RG equations. This result is in agreement with the recent calculation by Verma [10], where it was shown that  $B_0 = \text{constant}$  does not satisfy RG equations, but the renormalized mean magnetic field ( $B_0 \propto k^{-1/3}$ ) and Kolmogorov's energy spectrum ( $k^{-5/3}$ ) do satisfy the RG equations. From these arguments we can claim that Kraichnan's 3/2 powerlaw is ruled out for strong MHD turbulence. However,  $k^{-3/2}$  may still be considered in the framework of weak turbulence theory.

In our calculation we take  $r_A(k) = E^u(k)/E^b(k)$  to be a constant. The global Alfvén ratio  $E^u/E^b$  may differ significantly from  $r_A(k)$ , still we make the approximation  $r_A(k) = r_A$  to simplify the calculation. Similarly we have assumed that  $\sigma_c(k) = \text{const} = \sigma_c$ . In addition we also assume isotropy which does not hold in the large  $r_A$  limit. It is hoped that future calculations will be able to relax these assumptions and attempt solutions for more realistic situations.

In many of the earlier RG calculations [1,4] it is assumed that the dynamical system under consideration is forced by random noise at all scales. In those calculations, the noise and the vertex (coefficient of the nonlinear term) usually get renormalized along with the renormalization of dissipative coefficients. In contrast, in our scheme only the dissipative constants are renormalized, and the renormalization correction to other parameters (e.g. noise) are implicitly lumped into the full correlation function by assuming Kolmogorov's powerlaw. Our procedure is relatively simple, and one can easily calculate various interesting quantities. We hope that future developments in dynamical RG will be able to justify some of the assumptions made in our procedure.

To conclude, we have applied RG procedure to MHD turbulence and calculated the renormalized viscosity and resistivity. These parameters find applications in simulations. We have shown that that Kolmogorov's spectrum is a consistent solution of MHD RG equation. The results presented here are in general agreement with the recent

EDQNM and numerical results. Validation of the results presented here with numerical simulations will give us important insights into physics of MHD turbulence.

### ACKNOWLEDGMENTS

The author thanks J. K. Bhattacharjee for valuable discussions and insights from the inception to the end of the problem. The author also benefitted greatly from the numerous discussions he had with G. Dar and V. Eswaran on simulation results.

### APPENDIX A: PERTURBATIVE CALCULATION OF MHD EQUATIONS

The MHD equations (2.4, 2.5) can be written as

$$\begin{pmatrix} u_i(\hat{k}) \\ b_i(\hat{k}) \end{pmatrix} = \begin{pmatrix} G^{uu}(\hat{k}) & G^{ub}(\hat{k}) \\ G^{bu}(\hat{k}) & G^{bb}(\hat{k}) \end{pmatrix} \begin{pmatrix} -\frac{i}{2}P_{ijm}^+(\mathbf{k}) \int d\hat{p} [u_j(\hat{p})u_m(\hat{k}-\hat{p}) - b_j(\hat{p})b_m(\hat{k}-\hat{p})] \\ -iP_{ijm}^-(\mathbf{k}) \int d\hat{p} [u_j(\hat{p})b_m(\hat{k}-\hat{p})] \end{pmatrix} \quad (\text{A1})$$

where the Greens function  $G$  can be obtained from  $G^{-1}(\hat{k})$

$$G^{-1}(k, \omega) = \begin{pmatrix} -i\omega - \Sigma^{uu} & \Sigma^{ub} \\ \Sigma^{bu} & -i\omega - \Sigma^{bb} \end{pmatrix}. \quad (\text{A2})$$

We solve the above equation perturbatively keeping the terms to the first order (nonvanishing). As usual, we represent the integrals by Feynmann diagrams. To the leading order, the quantities  $u_i$  and  $b_i$  are expanded as

$$u_i = \text{thick wiggly line} = G^{uu} \text{thick wiggly line} \begin{matrix} / u_j \\ \backslash u_m \end{matrix} - G^{uu} \text{thin wiggly line} \begin{matrix} / b_j \\ \backslash b_m \end{matrix} + G^{ub} \text{thin wiggly line} \begin{matrix} / u_j \\ \backslash b_m \end{matrix} + \dots \quad (\text{A3})$$

$$b_i = \text{dashed line} = G^{bu} \text{thick curly line} \begin{matrix} / u_j \\ \backslash u_m \end{matrix} - G^{ub} \text{thin curly line} \begin{matrix} / b_j \\ \backslash b_m \end{matrix} + G^{bb} \text{thin curly line} \begin{matrix} / u_j \\ \backslash b_m \end{matrix} + \dots \quad (\text{A4})$$

The variables  $u$  and  $b$  are represented by solid and dashed line respectively. The quantity  $G^{uu}, G^{ub}, G^{bb}, G^{bu}$  are represented by thick wiggly (photon), thin wiggly, thick curly (gluon), and thin curly lines respectively. The filled circle represents  $(-i/2)P_{ijm}^+$  vertex, while the empty circle represents  $-iP_{ijm}^-$  vertex.

The substitution of  $u_i^>$  and  $b_i^>$  in the second bracketed terms of Eqs. (2.13, 2.14), denoted by  $I_2^u$  and  $I_2^b$  respectively, will yield

$$I_2^u = 2 \begin{matrix} / > \\ \backslash < \end{matrix} \text{thick wiggly line} - 2 \begin{matrix} / > \\ \backslash < \end{matrix} \text{thin wiggly line} \quad (\text{A5})$$

$$I_2^b = \begin{matrix} / > \\ \backslash < \end{matrix} \text{thick curly line} + \begin{matrix} / < \\ \backslash > \end{matrix} \text{thin curly line} \quad (\text{A6})$$

We illustrate the expansion of one of the above diagrams:

$$\begin{matrix} / > \\ \backslash < \end{matrix} \text{thick wiggly line} = 2 \begin{matrix} \text{thick wiggly line} \\ \text{thick wiggly line} \end{matrix} \begin{matrix} / > \\ \backslash < \end{matrix} \text{thick wiggly line} + \begin{matrix} \text{thick wiggly line} \\ \text{thick wiggly line} \end{matrix} \begin{matrix} / < \\ \backslash > \end{matrix} \text{thin wiggly line} + \begin{matrix} \text{thick wiggly line} \\ \text{thick wiggly line} \end{matrix} \begin{matrix} / > \\ \backslash < \end{matrix} \text{thin wiggly line} + 2 \begin{matrix} \text{thick wiggly line} \\ \text{thick wiggly line} \end{matrix} \begin{matrix} / < \\ \backslash > \end{matrix} \text{thin wiggly line}$$

$$\begin{aligned}
& 2 \begin{array}{c} \text{diagram 1} \\ \langle \rangle \end{array} - \begin{array}{c} \text{diagram 2} \\ \langle \rangle \end{array} - \begin{array}{c} \text{diagram 3} \\ \langle \rangle \end{array} - 2 \begin{array}{c} \text{diagram 4} \\ \langle \rangle \end{array} + \\
& \begin{array}{c} \text{diagram 5} \\ \langle \rangle \end{array} + \begin{array}{c} \text{diagram 6} \\ \langle \rangle \end{array} + \begin{array}{c} \text{diagram 7} \\ \langle \rangle \end{array} + \begin{array}{c} \text{diagram 8} \\ \langle \rangle \end{array} + \\
& \begin{array}{c} \text{diagram 9} \\ \langle \rangle \end{array} + \begin{array}{c} \text{diagram 10} \\ \langle \rangle \end{array} + \begin{array}{c} \text{diagram 11} \\ \langle \rangle \end{array} + \begin{array}{c} \text{diagram 12} \\ \langle \rangle \end{array} \\
& \text{+higher order diagrams} \tag{A7}
\end{aligned}$$

In the above diagrams solid lines denote  $C^{uu}$ , and the dotted lines denote  $C^{ub}$ . The correlation function  $C^{bb}$  is denoted by dashed line. As mentioned earlier, the wiggly and curly lines denote various Green's functions. All the diagrams except 4,8,12, and 16th can be shown to be trivially zero using Eqs. (2.15–2.21). We assume that 4,8,12, and 16th diagrams are also zero, as usually done in turbulence RG calculations [4,5]. Similarly we can show that all other diagrams of  $I_2^u$  and  $I_2^b$  are zero, hence,  $I_2^u = I_2^b = 0$  to first order.

The third bracketed terms of (2.13, 2.14), denoted by  $I_3^u$  and  $I_3^b$  respectively, are diagrammatically represented as

$$\begin{aligned}
I_3^u &= \begin{array}{c} \text{diagram 13} \\ \text{diagram 14} \end{array} \\
&= -\delta\Sigma^{uu}(k) \begin{array}{c} \text{diagram 15} \\ \langle \rangle \end{array} - \delta\Sigma^{ub}(k) \begin{array}{c} \text{diagram 16} \\ \langle \rangle \end{array} \tag{A8}
\end{aligned}$$

$$\begin{aligned}
I_3^b &= \begin{array}{c} \text{diagram 17} \\ \text{diagram 18} \end{array} \\
&= -\delta\Sigma^{bu}(k) \begin{array}{c} \text{diagram 19} \\ \langle \rangle \end{array} - \delta\Sigma^{bb}(k) \begin{array}{c} \text{diagram 20} \\ \langle \rangle \end{array} \tag{A9}
\end{aligned}$$

where

$$-(d-1)\delta\Sigma^{uu} = 4 \begin{array}{c} \text{diagram 21} \\ \gg \end{array} - 2 \begin{array}{c} \text{diagram 22} \\ \gg \end{array} + 2 \begin{array}{c} \text{diagram 23} \\ \gg \end{array} - 4 \begin{array}{c} \text{diagram 24} \\ \gg \end{array} \tag{A10}$$

$$-(d-1)\delta\Sigma^{ub} = -4 \begin{array}{c} \text{diagram 25} \\ \gg \end{array} + 2 \begin{array}{c} \text{diagram 26} \\ \gg \end{array} + 4 \begin{array}{c} \text{diagram 27} \\ \gg \end{array} - 2 \begin{array}{c} \text{diagram 28} \\ \gg \end{array} \tag{A11}$$

$$-(d-1)\delta\Sigma^{bu} = 2 \begin{array}{c} \text{diagram 29} \\ \gg \end{array} + \begin{array}{c} \text{diagram 30} \\ \gg \end{array} + \begin{array}{c} \text{diagram 31} \\ \gg \end{array} - 2 \begin{array}{c} \text{diagram 32} \\ \gg \end{array} \tag{A12}$$

$$-(d-1)\delta\Sigma^{bb} = 2 \begin{array}{c} \text{diagram 33} \\ \gg \end{array} + \begin{array}{c} \text{diagram 34} \\ \gg \end{array} + \begin{array}{c} \text{diagram 35} \\ \gg \end{array} - \begin{array}{c} \text{diagram 36} \\ \gg \end{array} \tag{A13}$$

In Eqs. (A10–A13) we have omitted all the vanishing diagrams (similar to those appearing in  $I_2$ ). Looking at the all the terms, we observe  $I_3^u$  contributes to  $\Sigma^{uu}$  and  $\Sigma^{ub}$  renormalization, while  $I_3^b$  contributes  $\Sigma^{bb}$  and  $\Sigma^{bu}$  renormalization. The algebraic expressions for the above diagrams are given by Eqs. (2.24–2.27).

## APPENDIX B: VALUES OF $S_I$

$S_i(k, p, q)$  are formed by contracting tensors  $P_{ijm}^+, P_{ijm}^-, P_{ij}$  and  $M_{ijm}$  (see Eqs. (2.8,2.10,3.2)). On simplification  $S_i$ s become functions of  $k, p, q$  and cosines  $x, y, z$  defined as

$$\mathbf{p} \cdot \mathbf{q} = -pqx; \quad \mathbf{q} \cdot \mathbf{k} = qky; \quad \mathbf{p} \cdot \mathbf{k} = pkz. \quad (\text{B1})$$

The algebraic expressions for various  $S_i(k, p, q)$  are given below.

$$\begin{aligned} S_1(k, p, q) &= M_{bjm}(k)M_{mab}(p)P_{ja}(q) \\ &= kp(d-2+z^2)(z+xy) \end{aligned} \quad (\text{B2})$$

$$\begin{aligned} S_2(k, p, q) &= M_{ajm}(k)M_{mab}(p)P_{jb}(q) \\ &= kp(-z+z^3+y^2z+xyz^2) \end{aligned} \quad (\text{B3})$$

$$\begin{aligned} S_3(k, p, q) &= M_{bjm}(k)M_{jab}(p)P_{ma}(q) \\ &= kp(-z+z^3+x^2z+xyz^2) \end{aligned} \quad (\text{B4})$$

$$\begin{aligned} S_4(k, p, q) &= M_{ajm}(k)M_{jab}(p)P_{mb}(q) \\ &= kp(-z+z^3+xy+x^2z+y^2x+xyz^2) \end{aligned} \quad (\text{B5})$$

$$\begin{aligned} S(k, p, q) &= P_{bjm}^+(k)P_{mab}^+(p)P_{ja}(q) \\ &= kp((d-3)z+2z^3+(d-1)xy) \end{aligned} \quad (\text{B6})$$

$$\begin{aligned} S_5(k, p, q) &= P_{bjm}^+(k)P_{mab}^-(p)P_{ja}(q) \\ &= kp((d-1)z+(d-3)xy-2y^2z) \end{aligned} \quad (\text{B7})$$

$$\begin{aligned} S_6(k, p, q) &= P_{ajm}^+(k)P_{mba}^-(p)P_{jb}(q) \\ &= -S_5(k, p, q) \end{aligned} \quad (\text{B8})$$

$$\begin{aligned} S_7(k, p, q) &= P_{ijm}^-(k)P_{mab}^+(p)P_{ja}(q)P_{ib}(k) \\ &= S_5(p, k, q) \end{aligned} \quad (\text{B9})$$

$$\begin{aligned} S_8(k, p, q) &= P_{ijm}^-(k)P_{jab}^+(p)P_{ma}(q)P_{ib}(k) \\ &= -S_5(p, k, q) \end{aligned} \quad (\text{B10})$$

$$\begin{aligned} S_9(k, p, q) &= P_{ijm}^-(k)P_{mab}^-(p)P_{ja}(q)P_{ib}(k) \\ &= kp(d-1)(z+xy) \end{aligned} \quad (\text{B11})$$

$$\begin{aligned} S_{10}(k, p, q) &= P_{ijm}^-(k)P_{mab}^-(p)P_{jb}(q)P_{ia}(k) \\ &= -S_9(k, p, q) \end{aligned} \quad (\text{B12})$$

$$\begin{aligned} S_{11}(k, p, q) &= P_{ijm}^-(k)P_{jab}^-(p)P_{ma}(q)P_{ib}(k) \\ &= -S_9(k, p, q) \end{aligned} \quad (\text{B13})$$

$$\begin{aligned} S_{12}(k, p, q) &= P_{ijm}^-(k)P_{jab}^-(p)P_{mb}(q)P_{ia}(k) \\ &= S_9(k, p, q) \end{aligned} \quad (\text{B14})$$

There are many useful relationships between  $S_i(k, p, q)$ s. Some of them are

$$S(k, p, q) = S_1(k, p, q) + S_2(k, p, q) + S_3(k, p, q) + S_4(k, p, q) \quad (\text{B15})$$

$$S_5(k, p, q) = S_1(k, p, q) - S_2(k, p, q) + S_3(k, p, q) - S_4(k, p, q) \quad (\text{B16})$$

[1] D. Forster, D. R. Nelson, and M. J. Stephen, Phys. Rev. A **16**, 732 (1977).

[2] C. DeDominicis and P. C. Martin, Phys. Rev. A **19**, 419 (1979).

[3] J. D. Fournier and U. Frisch, Phys. Rev. A **17**, 747 (1979).

- [4] V. Yakhot and S. A. Orszag, *J. Sci. Comput.* **1**, 3 (1986).
- [5] W. D. McComb, *The Physics of Fluid Turbulence* (Clarendon, Oxford, 1990).
- [6] W. D. McComb, *Rep. Prog. Phys.* **58**, 1117 (1995).
- [7] J. D. Fournier, P.-L. Sulem, and A. Pouquet, *J. Phys. A* **15**, 1393 (1982).
- [8] S. J. Camargo and H. Tasso, *Phys. Fluids B* **4**, 1199 (1992).
- [9] W. Z. Liang and P. H. Diamond, *Phys. Fluids B* **5**, 63 (1993).
- [10] M. K. Verma, *Phys. Plasma* **6**, 1455 (1999).
- [11] R. H. Kraichnan, *Phys. Fluids* **8**, 1385 (1965).
- [12] P. S. Iroshnikov, *Sov. Astron. I.* **7**, 566 (1964).
- [13] W. H. Matthaeus and Y. Zhou, *Phys. Fluids B* **1**, 1929 (1989).
- [14] Y. Zhou and W. H. Matthaeus, *J. Geophys. Res.* **95**, 10291 (1990).
- [15] E. Marsch, in *Reviews in Modern Astronomy*, edited by G. Klare (Springer-Verlog, Berlin, 1990), p. 43.
- [16] W. H. Matthaeus and M. L. Goldstein, *J. Geophys. Res.* **87**, 6011 (1982).
- [17] E. Marsch and C.-Y. Tu, *J. Geophys. Res.* **95**, 8211 (1990).
- [18] M. K. Verma, D. A. Roberts, and M. L. Goldstein *et al.*, *J. Geophys. Res.* **101**, 21619 (1996).
- [19] W. C. Müller and D. Biskamp, *Phys. Rev. Lett.* **84**, 475 (2000).
- [20] D. Biskamp and W. C. Müller, *Phys. Plasma* **7**, 4889 (2000).
- [21] S. Sridhar and P. Goldreich, *Astrophys. J.* **432**, 612 (1994).
- [22] P. Goldreich and S. Sridhar, *Astrophys. J.* **438**, 763 (1995).
- [23] J. D. Fournier, U. Frisch, and A. Rose, *J. Phys. A* **11**, 187 (1978).
- [24] W. D. McComb and A. G. Watt, *Phys. Rev. A* **46**, 4797 (1992).
- [25] Y. Zhou and G. Vahala, *Phys. Rev. E* **47**, 2503 (1993).
- [26] A. Pouquet, *J. Fluid Mech.* **88**, 1 (1994).
- [27] A. Ishizawa and Y. Hattori, *J. Phy. Soc. Jpn.*, **67**, 4302, (1998).
- [28] A. Ishizawa and Y. Hattori, *J. Phy. Soc. Jpn.* **67**, 441 (1998).
- [29] G. Dar, M. K. Verma, and V. Eswaran, *Physica D*, **157**, 207, 2001.
- [30] M. K. Verma and J. K. Bhattacharjee, *Europhys. Lett.* **31**, 195 (1995).

## Figure Captions

**Fig. 1.** Plot of  $\nu^*(k')$  (solid) and  $\eta^*(k')$  (dashed) vs.  $k'$  for  $d = 3$  and  $\sigma_c = 0, r_A = 1$ . Values at various iterations are shown by different curves.

**Fig. 2.** Plot of  $\nu^*(k')$  and  $\eta^*(k')$  vs.  $k'$  for  $d = 2$  and  $\sigma_c = 0, r_A = 1$ .

**Fig. 3.** Plot of asymptotic  $\nu^*$  (square) and  $\eta^*$  (diamond) vs.  $d$  for  $\sigma_c = 0$  and  $r_A = 1$ . The fluid  $\nu^*$  (triangle) is also plotted for reference. The solid lines are the  $d^{-1/2}$  curves.

TABLE I. The values of  $\nu^*$ ,  $\eta^*$ ,  $\nu^{uu^*}$ ,  $\nu^{ub^*}$ ,  $\eta^{bu^*}$ ,  $\eta^{bb^*}$  for various space dimensions  $d$  with  $r_A = 1$  and  $\sigma_c = 0$ .

$d$	$\nu^*$	$\eta^*$	$Pr$	$\nu^{uu^*}$	$\nu^{ub^*}$	$\eta^{bu^*}$	$\eta^{bb^*}$
2.1	--	--	--	--	--	--	--
2.2	1.9	0.32	6.0	-0.041	1.96	-0.44	0.76
2.5	1.2	0.57	2.1	0.089	1.15	-0.15	0.72
3.0	1.00	0.69	1.4	0.20	0.80	0.078	0.61
4.0	0.83	0.70	1.2	0.27	0.56	0.21	0.49
7.0	0.62	0.59	1.1	0.26	0.36	0.25	0.34
10.0	0.51	0.50	1.0	0.23	0.28	0.22	0.28
50.0	0.23	0.23	1.0	0.11	0.12	0.11	0.12
100	0.14	0.14	1.0	0.065	0.069	0.066	0.069

TABLE II. The values of  $\nu^*$ ,  $\eta^*$ ,  $\nu^{uu^*}$ ,  $\nu^{ub^*}$ ,  $\eta^{bu^*}$ ,  $\eta^{bb^*}$  for various  $r_A$  when  $d = 3$  and  $\sigma_c = 0$ .

$r_A$	$\nu^*$	$\eta^*$	$Pr$	$\nu^{uu^*}$	$\nu^{ub^*}$	$\eta^{bu^*}$	$\eta^{bb^*}$
$\infty$	0.38	--	--	0.38	--	--	--
5000	0.36	0.85	0.42	0.36	1.4E-4	-0.023	0.87
100	0.36	0.85	0.42	0.36	7.3E-3	-0.022	0.87
5	0.47	0.82	0.57	0.32	0.15	-4.7E-4	0.82
2	0.65	0.78	0.83	0.27	0.38	0.031	0.75
1	1.00	0.69	1.4	0.20	0.80	0.078	0.61
0.5	2.1	0.50	4.2	0.11	2.00	0.15	0.35
0.3	11.0	0.14	78	0.022	11.0	0.082	0.053
0.2	--	--	--	--	--	--	--



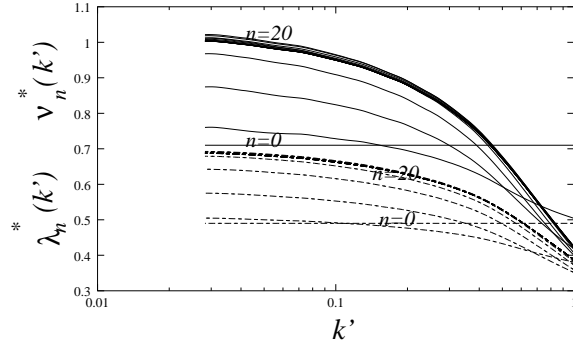


FIG. 1. Plot of  $\nu^*(k')$  (solid) and  $\eta^*(k')$  (dashed) vs.  $k'$  for  $d = 3$  and  $\sigma_c = 0, r_A = 1$ . Values at various iterations are shown by different curves.

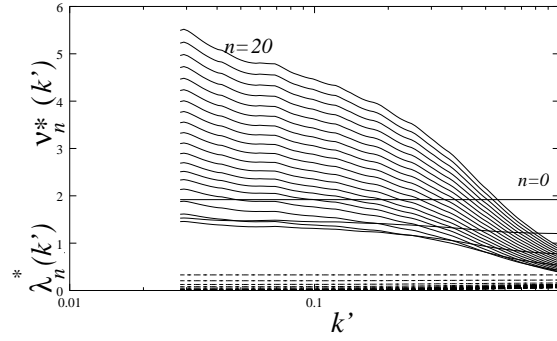


FIG. 2. Plot of  $\nu^*(k')$  and  $\eta^*(k')$  vs.  $k'$  for  $d = 2$  and  $\sigma_c = 0, r_A = 1$ .

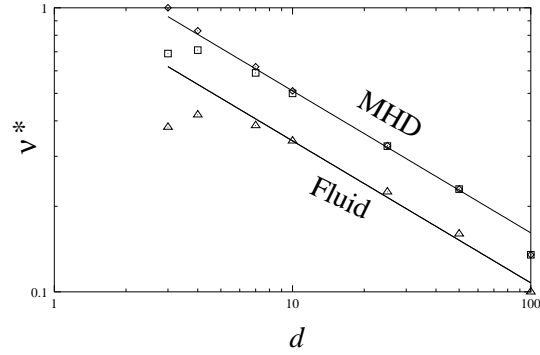


FIG. 3. Plot of asymptotic  $\nu^*$  (square) and  $\eta^*$  (diamond) vs.  $d$  for  $\sigma_c = 0$  and  $r_A = 1$ . The fluid  $\nu^*$  (triangle) is also plotted for reference. The solid lines are the  $d^{-1/2}$  curves .